Alexandria Engineering Journal (2022) xxx, xxx–xxx

HOSTED BY

ELSEVIER

Alexandria University

Alexandria Engineering Journal

www.elsevier.com/locate/aej
www.sciencedirect.com

Flow of hybrid CNTs past a rotating sphere subjected to thermal radiation and thermophoretic particle deposition

G.K. Ramesh [a,1], J.K. Madhukesh [b], Nehad Ali Shah [c,1], Se-Jin Yook [d,*]

[a] *Department of Mathematics, K.L.E. Society's J.T. College, Gadag 582101, Karnataka, INDIA*
[b] *Department of Mathematics, Davangere University, Davangere 577002, Karnataka, INDIA*
[c] *Department of Mechanical Engineering, Sejong University, Seoul 05006, South Korea*
[d] *School of Mechanical Engineering, Hanyang University, 222 Wangsimni-ro, Seongdong-gu, Seoul 04763, Republic of Korea*

Received 15 June 2022; revised 17 August 2022; accepted 11 September 2022

KEYWORDS

Hybrid nanofluid;
Carbon nanotubes;
Thermal radiation;
Thermophoretic particle deposition;
Rotating sphere

Abstract Thermal radiation and thermophoretic particle deposition have important applications in research and engineering. These two principles are employed in practical applications such as electrical fuel, projectiles, thermal transportation, renewable energy, nuclear power plants, gas turbines, and aerospace engineering. In light of the aforementioned applications, the current study investigates the stagnation point hybrid CNTs movement around a rotating sphere in the existence of thermal radiation and thermophoretic particle deposition. Using appropriate similarity factors, nonlinear governing equations are converted into ordinary differential equations. The Runge Kutta Fehlberg 45 (RKF-45) order and a shooting approach are used to find the numerical results of the simplified equations and boundary conditions. The numerical findings are presented graphically. It is explored how different limitations impact their individual profiles. According to the research, primary velocity increases with acceleration parameter but decreases with secondary velocity. As the radiation parameter value increases, so does the thermal distribution. Concentration decreases as both the Schmidt number and the thermophoretic parameter decrease. The heat dispersion rate heightens as the percentage of volume fraction of solid and the radiation parameter increase. Mano CNTs have a higher primary velocity than hybrid CNTs.

1. Introduction

Due to its huge variety of relevance in biomedicine, thermal exchangers, freezing of electrical devices, double windowpane, food, shipping, and so on, the notion of nanoliquids has become a broader subject for researchers in recent years. To upsurge the thermal conductivity of common liquids such as

* Corresponding author.
E-mail addresses: gkrmaths@gmail.com (G.K. Ramesh), madhukeshjk@gmail.com (J.K. Madhukesh), nehadali199@sejong.ac.kr (N. Ali Shah), ysjnuri@hanyang.ac.kr (S.-J. Yook).

[1] These authors contributed equally to this work and are co-first authors.

Peer review under responsibility of Faculty of Engineering, Alexandria University.

https://doi.org/10.1016/j.aej.2022.09.026

Nomenclature

A	Acceleration parameter
C_W	Well concentration
C_1	Concentration
C_∞	Ambient concentration
Cf_x, Cf_z	Skin friction along x&z directions
D	Diffusivity
$f(\eta)$	Primary velocity profile
$g(\eta)$	Secondary velocity profile
k	Thermal conductivity
k^*	Mean absorption coefficient
K_2^*	Thermophoretic constant
Nu	Nusselt number
Pr	Prandtl number
q_r	Radiation heat flux

Greek letters

ρ	Density
v	Kinematic viscosity
ρC_p	Heat capacitance
σ^*	Stefan-Boltzmann Coefficient
λ	Rotation parameter
η	Similarity variable

Subscript

hnf	Hybrid nanofluid
f	Fluid
$SWCNT$	Single wall carbon nanotube
$r_1(x_1)$	radial distance from a surface element to the axis of symmetry
R_{ad}	Radiation parameter
Re	Local Reynolds number
Sh	Sherwood number
Sc	Schmidt number
t	time
T_r	Reference temperature
T_1	Temperature
T_W	Wall temperature
T_∞	For field temperature
V_{T1}	Thermophoretic velocity
u_1, v_1, w_1	Velocity components
x_1^*, y_1^*, z_1^*	The Coordinates of a sphere
$\Omega(t)$	angular velocity
$\theta(\eta)$	Dimensionless temperature profile
$\chi(\eta)$	Dimensionless concentration profile
μ	Dynamic viscosity
τ	Thermophoretic parameter
nf	Nanofluid
$MWCNT$	Multi-wall carbon nanotube

ethylene glycol, water, motor oils, and kerosene, various kinds of nanoparticles such as silica, silver, gold, alumina, copper, graphene, carbon nanotubes, and so on must be added to the base fluids. In 1995, Choi [1] proposed the properties of thermal conductivity and temperature distribution using nanofluids. Here are some of the noticeable works on nanofluid. In the context of the darcy-forchheimer and lorentz factors, Rasool et al. [2] looked into the effects of Rosseland's radiative activity on a responsive maxwell nanofluid stream across an isothermally warmed stretched sheet. In a Riga surface with a heat source/sink, Madhukesh et al. [3] investigated the nature of SWCNT/H_2O nano sized particles and moving microorganisms. Three distinct kinds of nano fluids were deliberated by Khan et al. [4] using the C-C heat flow model and the OHAM evaluation. Stalin et al. [5] examined the thermal characteristics of CeO_2/water-based nanofluids for thermal transport applications. In the influence of chemically reactive activation energy, Madhukesh et al. [6] investigated the Bio-Marangoni convection movement of Casson nano liquid across a porous medium. Hybrid nanofluids are a unique class of colloidal fluids that have piqued the interest of researchers due to the possible customization of their thermo-physical characteristics for heat transfer augmentation by combining more than one nano-additive to fulfill specific application needs. A hybrid nanofluid improves heat transmission more than a mono-nanofluid, which is significant in applications where temperature distribution is critical, such as electronic cooling, heat exchangers, pool boiling, and so on. Recently, Ramesh et al. [7] investigated crosswise and streamwise aspects of activation energy and covalent bonding procedure in the movement of a hybrid liquid over a heated plate. Magneto hydrodynamic flow of Cu-Al2O3/Water based hybrid nano liquid flow in a permeable channel was examined by Das et al. [8]. Salehi et al. [9] examined hydrothermal examination of MHD squeezing mixed liquid suspended with hybrid nano sized particles among two equivalent plates. Nayak et al. [10] inspected thermofluidic consequence of non-Newtonian liquid with hybrid nano structures. Cross hybrid nanofluid hydromagnetic flow and thermal interpretations impacted by three kinds of thermal radiations for any Prandtl values were inspected by Shaw et al. [11]. Hosseinzadeh et al. [12] deliberated the entropy production in a 3-D Bödewadt movement of water and hexanol type of base liquid containing Fe3O4 and MoS2 hybrid nano sized particles. The bioconvection of a radiating nano liquid via a fine needle in the context of a heterogeneous-homogeneous chemical process was discussed by Puneeth et al. [13]. A thermal investigation of a moving porous fin saturated with a hybrid nano liquid and having concave parabolic, trapezoidal, and convex cross sections were made by Hosseinzadeh et al. [14].

Because of their large surface area and high absorbance capability, carbon-based nanoparticles can make significant contributions to the environment and agriculture. Carbon-based nanoparticles are classified into different categories based on the form of the nanoparticles, which might be spherical or ellipsoids, spires, or tubes. Depending on the number of concentric films of folded graphene surface, CNTs are further classified as single-wall carbon nanotubes (SWCNTs) or multi-wall carbon nanotubes (MWCNTs). Many works are carried out on the concept of carbon nanotubes. Recently, the Simultaneous impact of the hall and wall properties in peristaltic convective carbon–water flow exposed to soret and Dufour

phenomena were investigated by Hussain and Muhammad [15]. Iqbal et al. [16] conducted a computational investigation of the effect of carbon nanotubes on heat transfer in MHD nanofluid flow across a stretchy spinning disc. Madhukesh et al. [3] deliberate the behavior of water-carrying SWCNT nanomaterials and moving microorganisms over a Riga surface with a heat source/sink. Different base fluids suspended by CNTs hybrid nanoparticles over a vertical circular cylinder with a sinusoidal radius were investigated by Gholinia et al. [17].

Thermal radiation (T-R) is electromagnetic radiation released by a substance as a result of its heat, the properties of which vary on the temperature of the material. Thermal radiation heats up by raising thermal diffusivity. The outcomes of thermal radiation are often used in commercial and high-temperature applications such as electrical energy, food, solar energy panels, projectiles, nuclear power plants, gas turbines, and aerospace engineering. Thermal radiation effects may be crucial in maintaining heat transfer in the polymer processing industries, where the final product's quality is altered by heat-controlling variables to some extent. The influence of radiation and magnetic field on the optimization of hybrid nanoparticles with mixed fluid flow in an octagonal porous media was inspected by Hosseinzadeh et al. [18]. Gireesha et al. [19] scrutinized magnetized Carreau fluid movement over a penetrable sensor surface with T-R, joule heating, and heat generation effects. Hosseinzadeh et al. [20] inspected the Nano-Bioconvective fluid motile microbe and nanoparticle flow investigation using MHD and heat radiation. Shah et al. [21] examined the numerical simulation of a thermally enhanced EMHD flow of a heterogeneous micropolar mixture comprising (60%)-ethylene glycol (EG), (40%)-water (W), and copper oxide nanomaterials (CuO).

Thermophoresis is the movement of minute particles away from a warmer object and toward a cooler one. The thermophoresis mechanism alerts the system when micro-sized constituents accelerate in the direction of dropping temperature gradients and are suspended in non-isothermal gas. The importance of theoretical and experimental knowledge of thermophoretic particle deposition cannot be overstated. TPD in the flow of fluid plays a key function in a variety of industrial and heat engineering applications such as air purifiers, powdered coal burners, building ventilation systems, and heat transfer. In the occurrence of T-P-D impact, Green and Lane [22] and Fuchs [23] both described how to use the current approach in practice. Goren [24] was the first to investigate T-P-D. Raju et al. [25] examined the nonlinear movements of axisymmetric ternary hybrid nanofluids in a thermally radiated expanding or contracting permeable Darcy Walls with different shapes and densities: Simple linear regression. Chen et al. [26] explored T-P-D in the stream of a dual stratified Casson fluid including a magnetic dipole and extended Fourier's and Fick's equations. Shankaralingappa et al. [27] evaluated the effect of T-P-D on the three-dimensional flow of Sodium Alginate-based Casson nanofluid across a extending surface.

For a variety of engineering activities, such as re-entry of ballistic, fibre coating, motion of projectile, and designing of rotating equipment, the rotational outflows and heat transfer elements of a driven movement of stream across stationary spinning bodies of circulation are significant. The heat transfer across a liquid movement and a rotating sphere has various technological uses, including overcoming freezing malfunctions. A blood-based hybrid nano liquid's mixed convection stagnation point circulation around a revolving sphere was studied by Gul et al. [28]. Malvandi [29] inspected the unsteady movement of a nanofluid in a time-dependent spinning sphere's stagnation point region. In the stagnation point zone of a revolving sphere, Anilkumar and Roy [30] explored into the self-similar solutions of an inconsistent mixed convection flow. Mahdy et al. [31] studied the Casson nano liquid's entropy assessment and unsteady MHD mixed convection stagnation-point motion around a rotational sphere. Sarkar and Kundu [32] discuss the impact of Hall current on the MHD unsteady movement of nano liquid on a rotating spherical body by considering solar radiation.

Based on the above-served literature, no work is done on stagnation point hybrid CNTs flow over a rotating sphere in the attendance of thermal radiation (T-R) and thermophoretic particle deposition. The purpose of the current inquiry is to discover the responses to the questions listed below.

1. What is the behavior of acceleration parameter over primary, secondary velocity, temperature, and concentration profiles in the presence of SWCNT/MWCNT nanoparticles.
2. When the thermal radiation constraint is improved, which kind of thermal performance is observed.
3. How does the concentration profile respond to thermophoretic constraint?.

2. Mathematical modeling:

Consider the incompressible, unsteady boundary layer flow of hybrid CNTs impending the forward stagnation point region of a persistent temperature rotating sphere in the presence of thermal radiation and thermophoretic particle deposition (Fig. 1). The x_1^* coordinate is represented on the surface and y_1^* is normal to the sphere. The sphere is rotating with angular velocity around a diameter that is parallel to the ambient velocity of the free stream (time-dependent)$\Omega(t) = Bt^{-1}, B > 0$. Before the time, the angular velocity of the sphere has no motion in the fluid. It is presumable that the temperature close to the wall is constant. Additionally, the parameters for viscous dissipation are negligible and the free stream and angular velocities rely on time in the

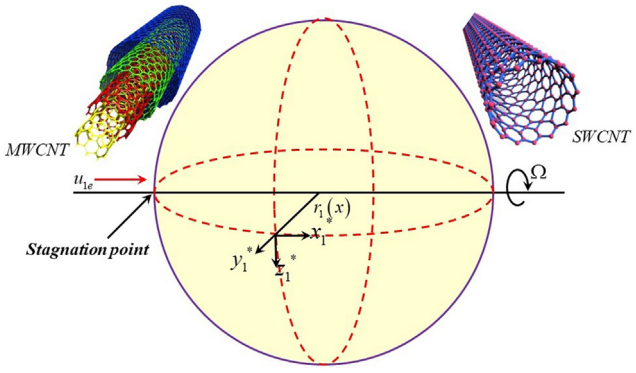

Fig. 1 Flow geometry.

form of$u_{1e}(x_1^*,t)=x_1^*At^{-1}$,$A>0$.The hybrid CNTs are in the thermal equilibrium state. T_W&T_∞ stands for the temperature at the sphere's wall and its ambient temperature, respectively. Also, for concentration it isC_W&C_∞. Based on the aforementioned premises, the problem is represented by the following mathematical model: (see [28-32,33]).

$$\frac{\partial(r_1u_1)}{\partial x_1^*}=-\frac{\partial(r_1v_1)}{\partial y_1^*}, \tag{1}$$

$$\frac{\partial u_1}{\partial t}+u_1\frac{\partial u_1}{\partial x_1^*}+v\frac{\partial u_1}{\partial y_1^*}=\left(\frac{w_1^2}{r_1}\right)\frac{dr_1}{dx_1^*}+u_e\frac{\partial u_e}{\partial x^*}+\frac{\partial u_e}{\partial t}+\nu_{hnf}\times\frac{\partial^2 u}{\partial y_1^2}, \tag{2}$$

$$\frac{\partial w_1}{\partial t}+u_1\frac{\partial w_1}{\partial x_1^*}+v_1\frac{\partial w_1}{\partial y_1^*}=\nu_{hnf}\frac{\partial^2 w_1}{\partial y_1^2}-\left(\frac{u_1w_1}{r_1}\right)\frac{dr_1}{dx_1^*}, \tag{3}$$

$$\frac{\partial T_1}{\partial t}+u\frac{\partial T_1}{\partial x_1^*}+v\frac{\partial T_1}{\partial y_1^*}=\frac{k_{hnf}}{(\rho C_p)_{hnf}}\frac{\partial^2 T_1}{\partial y_1^*}-\frac{1}{(\rho C_p)_{hnf}}\frac{\partial q_r}{\partial y_1^*}, \tag{4}$$

$$\frac{\partial C_1}{\partial t}+u\frac{\partial C_1}{\partial x_1^*}+v\frac{\partial C_1}{\partial y_1^*}=D_f\frac{\partial^2 C_1}{\partial y_1^2}-\frac{\partial(V_{T1}(C_1-C_\infty))}{\partial y_1^*}. \tag{5}$$

Subject to the initial and boundary conditions:

$$\begin{gathered}u_1(0,xv,y_1^*)=u_{1i}(x_1^*,y_1^*),\quad v_1(0,x_1^*,y_1^*)=v_{1i}(x_1^*,y_1^*)\\ w_1(0,x_1^*,y_1^*)=w_{1i}(x_1^*,y_1^*),\\ T_1(0,x_1^*,y_1^*)=T_{1i}(x_1^*,y_1^*),C_1(0,x_1^*,y_1^*)=C_{1i}(x_1^*,y_1^*)\end{gathered} \tag{6}$$

$$\begin{gathered}u_1(t,x_1^*,0)=0,\quad v_1(t,x_1^*,0)=0,\quad w_1(t,x_1^*,0)=\Omega(t)r_1,\\ T_1(t,x_1^*,0)=T_w,\\ w_1(t,x_1^*,\infty)=0,\quad u_1(t,x_1^*,w_1)=u_{1e}(x_1^*,t)=Ax_1^*/t,\\ T_1(t,x_1^*,\infty)=T_\infty,\quad C_1(t,x_1^*,\infty)=C_\infty.\end{gathered} \tag{7}$$

The thermophoretic velocity is defined using the work of [33] as.

$$V_{T1}=-\nu_f K_2^* T_r^{-1}\frac{\partial T_1}{\partial y_1^*} \tag{8}$$

Here, K_2^*&T_r^{-1} denotes thermophoretic constant and reference temperature.

The radiation heat flux term q_r present in equation number (4) is defined by the use of Rosseland's assumptions as.

$$q_r=\frac{4}{3}\left(\partial T_1^4/\partial y_1^*\right)\frac{\sigma^*}{k^*} \tag{9}$$

In the above equation, the term T_1^4 is a linear function of the temperature. By expanding the term T_1^4 up to infinity, we get.

$$T_1^4=T_\infty^4+4T_\infty^3(T_1-T_\infty)+6T_\infty^2(T_1-T_\infty)^2+\ldots \tag{10}$$

Expect the first degree $(T-T_\infty)$ by disregarding the higher-order components in the preceding equation. we obtain.

$$T_1^4\simeq 4T_\infty^3T_1-3T_\infty^4 \tag{11}$$

Substituting in the q_r expression, we obtain.

$$q_r=-\frac{16}{3}\left(\partial T_1/\partial y_1^*\right)\frac{\sigma^*T_\infty^3}{k^*} \tag{12}$$

By substituting the above expression into equation (4). It reduces into.

$$\frac{\partial T_1}{\partial t}+u\frac{\partial T_1}{\partial x_1^*}+v\frac{\partial T_1}{\partial y_1^*}=\left(\frac{k_{hnf}}{(\rho C_p)_{hnf}}+\frac{16}{3}\frac{\sigma^*T_\infty^3}{k^*(\rho C_p)_{hnf}}\right)\frac{\partial^2 T_1}{\partial y} \tag{13}$$

$$\begin{gathered}r_1\approx x_1^*,\quad \frac{dr_1}{dx}=1,\quad \eta=\frac{1}{\sqrt{\nu_f t}}y_1^*,\quad w=\frac{Bx_1^*}{t}g(\eta)\\ \psi=Ax_1^*\left(\frac{\nu_f}{t}\right)^{1/2}f(\eta),\quad \theta(\eta)=\frac{T_1-T_\infty}{T_w-T_\infty},\quad \chi(\eta)=\frac{C_1-C_\infty}{C_w-C_\infty}\end{gathered} \tag{14}$$

The thermophysical properties of CNTs are given as (see [34,35]).

$$\mu_{hnf}=\mu_f\frac{(1-\phi_1)^{-2.5}}{(1-\phi_2)^{2.5}}$$

$$\rho_{hnf}=\phi_2\rho_{MWCNT}+\{(1-\phi_1)\rho_f+\phi_1\rho_{SWCNT}\}(1-\phi_2)$$

$$(\rho C_p)_{hnf}=\phi_2(\rho C_p)_{MWCNT}+\left\{(1-\phi_1)(\rho C_p)_f+\phi_1(\rho C_p)_{SWCNT}\right\}(1-\phi_2)$$

$$\frac{k_{hnf}}{k_{nf}}=\frac{2\phi_2\left(\frac{k_{MWCNT}}{k_{MWCNT}-k_{nf}}\right)\ln\left(\frac{k_{MWCNT}+k_{nf}}{2k_{nf}}\right)+(1-\phi_2)}{2\phi_2\left(\frac{k_{nf}}{k_{MWCNT}-k_{nf}}\right)\ln\left(\frac{k_{MWCNT}+k_{nf}}{2k_{nf}}\right)+(1-\phi_2)}$$

$$\frac{k_{nf}}{k_f}=\frac{2\phi_1\left(\frac{k_{SWCNT}}{k_{MwCNT}-k_f}\right)\ln\left(\frac{k_{SWCNT}+k_f}{2k_f}\right)+(1-\phi_1)}{2\phi_1\left(\frac{k_f}{k_{SWCNT}-k_f}\right)\ln\left(\frac{k_{SWCNT}+k_f}{2k_f}\right)+(1-\phi_1)}$$

After simplification of governing equations, we obtain.

$$f'''+A_1A_2\left[f'-A(f')^2+f''\left(\frac{\eta}{2}+fA\right)+A(\lambda g^2+1)-1\right]=0 \tag{15}$$

$$g''+A_1A_2\left[g(1-2Af')+g'\left(\frac{\eta}{2}+fA\right)\right]=0 \tag{16}$$

$$\left(\frac{k_{hnf}}{k_f}+\frac{4R_{ad}}{3}\right)\frac{\theta''}{A_3}+\mathrm{Pr}\theta'\left[\frac{\eta}{2}+fA\right]=0 \tag{17}$$

$$\chi''+Sc\,\chi'\left[\frac{\eta}{2}+fA\right]-\tau Sc(\chi\theta''+\chi'\theta')=0 \tag{18}$$

The transformed boundary conditions become:

$$\left.\begin{array}{l}at\ \ \eta=0:\ \ g=1,\ \ f=0,\ \ f'=0,\ \ \theta=1,\ \ \chi=1\\ as\ \ \eta\to\infty:\ \ f'=1,\ \ \theta=0,\ \ \chi=0,\ \ g=0\end{array}\right\} \tag{19}$$

Where-

$A_1=(1-\phi_1)^{2.5}(1-\phi_2)^{2.5}$,-

$A_2=\frac{\phi_2\rho_{MWCNT}}{\rho_f}+\left\{(1-\phi_1)+\frac{\phi_1\rho_{SWCNT}}{\rho_f}\right\}(1-\phi_2)$,-

$A_3=\frac{\phi_2(\rho C_p)_{MWCNT}}{(\rho C_p)_f}+\left\{(1-\phi_1)+\frac{\phi_1(\rho C_p)_{SWCNT}}{(\rho C_p)_f}\right\}(1-\phi_2)$,

$\lambda=\left(\frac{B}{A}\right)^2$ Rotation parameter, A is acceleration parameter, $\mathrm{Pr}=\frac{\mu_f C_p}{k_f}$ Prandtl number, $Sc=\frac{\nu_f}{D_f}$ the Schmidt number, $R_{ad}=\frac{4\sigma^*T_\infty^3}{kk^*}$ radiation parameter, $\tau=-K_2^*T_r^{-1}(T_w-T_\infty)$ Thermophoretic parameter.

The skin friction along the x&z direction is given as.

Table 1 Thermophysical features of base liquid and CNTs (see [29,30]).

	$C_p(J/kg\,K)$	$k(W/mK)$	Pr	$\rho(kg/m^3)$
SWCNT	425	6600	–	2600
H_2O	4179	0.613	6.2	997.1
MWCNT	796	3000	–	1600

Table 2 Comparison of$f''(0)$,$-g'(0)$ and $-\theta'(0)$ for numerous values of A in the absence of$\phi_1, \phi_2 \& R_{ad}$.

	Malvandi [29]	Present study	Malvandi [29]	Present study	Malvandi [29]	Present study
A	$f''(0)$	$f''(0)$	$-g'(0)$	$-g'(0)$	$-\theta'(0)$	$-\theta'(0)$
0.5	0.79913	0.79921	0.30339	0.30354	0.467648	0.467656
1	1.2828	1.28232	0.64579	0.64585	0.589527	0.589536
2	1.9172	1.91845	1.05415	1.05427	0.779526	0.779538

Table 3 Computational values ofC_{fx},C_{fz},Nu and Sh for hybrid CNTs with various values of dimensionless constraints($\phi_1 = \phi_2 = 0.01$).

λ	R_{ad}	Sc	τ	A	C_{fx}	C_{fz}	Nu	Sh
1	1	0.8	0.1	1	2.216533	1.761552	9.712996	1.728027
3					2.458457	2.523033	9.738541	1.734902
5					2.694552	3.126915	9.762932	1.741453
	0.5				2.216533	1.761552	9.529410	1.815085
	1				2.216533	1.761552	9.712996	1.728029
	1.5				2.216533	1.761552	9.903250	1.676001
		0.8			2.216533	1.761552	9.712996	1.728027
		1.0			2.216533	1.761552	9.712996	2.092115
		1.2			2.216533	1.761552	9.712996	2.455438
			0.1		2.216533	1.761552	9.712996	1.728027
			0.3		2.216533	1.761552	9.712996	2.277877
			0.6		2.216533	1.761552	9.712996	3.108938
				0.5	1.196893	0.968653	9.423777	1.615144
				1.0	2.216533	1.761552	9.712996	1.728027
				1.5	3.180637	2.492087	9.989700	1.828279

$$Cf_x = \frac{\mu_{hnf}}{\rho_f u_e^2}\left(\frac{\partial u}{\partial y}\right)_{y=0} \rightarrow \sqrt{Re}Cf_x = \frac{f''(0)a^{-0.5}}{A_1} \tag{20}$$

$$Cf_z = -\frac{\mu_{hnf}}{\rho_f u_e^2}\left(\frac{\partial u}{\partial y}\right)_{y=0} \rightarrow \sqrt{Re}Cf_z = -\frac{g'(0)a^{-0.5}\lambda^{0.5}}{A_1} \tag{21}$$

Nusselt number and Sherwood number are given as.

$$Nu = \frac{-x\left(k_{hnf} + \frac{16}{3}\frac{\sigma^* T_\infty^3}{k^*}\right)\left(\frac{\partial T}{\partial y}\right)_{y=0}}{k_f(T_w - T_\infty)} \rightarrow \frac{Nu}{\sqrt{Re}} = -\left(\frac{k_{hnf}}{k_f} + \frac{4}{3}R_{ad}\right)\frac{\theta'(0)}{a^{0.5}} \tag{22}$$

$$Sh = \frac{-xD_f\left(\frac{\partial C}{\partial y}\right)_{y=0}}{D_f(C_w - C_\infty)} \rightarrow \frac{Sh}{\sqrt{Re}} = -\chi'(0)a^{0.5} \tag{23}$$

Here, $Re = v_f^{-1}u_e x^*$ is the local Reynolds number.

3. Numerical scheme and validation:

We turn the reduced ODEs into first-order initial value problems to find the numerical results for the reduced ODEs with boundary conditions. By the use of the shooting method to deduct the missing boundary conditions and then the numerical solution is obtained by applying Runge Kutta Fehlberg 45 order practice with step size 0.1 and error tolerance 10^{-6}.

Let us take,

$$f = \Gamma_1, f' = \Gamma_2, f'' = \Gamma_3$$

$$g = \Gamma_4, g' = \Gamma_5$$

Table 4 Computational values ofC_{fx},C_{fz},Nu and Sh for Nano CNTs with various values of dimensionless constraints($\phi_1 = 0.01$).

λ	R_{ad}	Sc	τ	A	C_{fx}	C_{fz}	Nu	Sh
1	1	0.8	0.1	1	2.177061	1.732312	9.724379	1.752239
3					2.413511	2.480825	9.748143	1.759065
5					2.644310	3.074245	9.770851	1.765572
	0.5				2.177061	1.732312	9.544053	1.857985
	1				2.177061	1.732312	9.724379	1.752242
	1.5				2.177061	1.732312	9.913609	1.691759
		0.8			2.177061	1.732312	9.724379	1.752239
		1.0			2.177061	1.732312	9.724379	2.122268
		1.2			2.177061	1.732312	9.724379	2.491518
			0.1		2.177061	1.732312	9.724379	1.752239
			0.3		2.177061	1.732312	9.724379	2.349376
			0.6		2.177061	1.732312	9.724379	3.251597
				0.5	2.177061	1.732312	9.724379	2.950061
				1.0	2.177061	1.732312	9.724379	4.464578
				1.5	2.177061	1.732312	9.724379	5.993214

$$\theta = \Gamma_6, \theta' = \Gamma_7$$

$$\chi = \Gamma_8, \chi' = \Gamma_9$$

$$\Gamma_3' = -\left(A_1 A_2\left[f' - A(f')^2 + f''(\frac{\eta}{2} + fA) + A(\lambda\Gamma_4^2 + 1) - 1\right]\right) \tag{24}$$

$$\Gamma_5' = -A_1 A_2\left[\Gamma_4(1 - 2A\Gamma_2) + \Gamma_5(\frac{\eta}{2} + \Gamma_1 A)\right] \tag{25}$$

$$\Gamma_7' = -\mathrm{Pr}A_3/\left(\frac{k_{hnf}}{k_f} + \frac{4R_{ad}}{3}\right)\Gamma_7\left[\frac{\eta}{2} + \Gamma_1 A)\right] \tag{26}$$

$$\Gamma_9' = -Sc\,\chi'\left[\frac{\eta}{2} + \Gamma_1 A\right] - \tau Sc(\Gamma_8\Gamma_7' + \Gamma_9\Gamma_7) \tag{27}$$

The transformed boundary conditions become:

$$\left.\begin{array}{c}\Gamma_1(0) = 0,\ \ \Gamma_2(0) = 0,\ \ \Gamma_3(0) = \Omega_1, \Gamma_4(0) = 1,\ \Gamma_5(0) = \Omega_2\,, \\ \Gamma_6(0) = 1,\ \ \Gamma_7(0) = \Omega_3\,, \Gamma_8(0) = 1, \Gamma_9(0) = \Omega_4\end{array}\right\} \tag{28}$$

A comparison with available outcomes for the skin-friction coefficient $f''(0)$ for $\phi_1, \phi_2 \& R_{ad}$ are absent, with the results of Malvida [29] for several values of A is made and shown in Table 2 in order to validate the methodology used in this study and assess the accuracy of the current analysis. This exhibit a good level of agreement, which inspires confidence in the accuracy of the numerical results.

4. Results and discussion:

The influence of numerous dimensionless constraints that control the temperature, velocity and concentrations over a rotating sphere in the attendance of hybrid carbon nanotubes with stagnation point, thermal radiation and thermophoretic particle deposition is analyzed in the present section. The thermophysical features of base liquid and CNTs are shown in Table 1. The set of ODEs is solved numerically with the help of the RKF-45 process with the shooting procedure. The obtained results are shown with the help of graphs and also the numerical method is validated by the prevailing available literature (see Table 2). The impact of various constraints on the engineering factorsCf_x,Cf_z, Nu and Sh are presented in Table 3 and 4.

Fig. 2 displays the increasing velocity profile for increasing$A$. The reverse behaviour is seen in the case of the secondary velocity profile (see Fig. 3). As the acceleration constraint enhances, it enhances the u_{1e} increases velocity in the adjacent axis within the boundary layer as the thickness of the momentum boundary layer decreases. Thermal distribution declines as the acceleration constraint enhances is displayed in the Fig. 4. Heat flow also decreases as the thermal boundary layer's thickness decreases. The similar behaviour is also seen in the case of concentration profile (see Fig. 5). It is observed from the Figs. 2-4 that, in primary velocity profile nano CNT shows higher velocity than that of hybrid CNTs. The secondary velocity, thermal distribution and concentration is more in hybrid CNTs than single CNT.

The nature of rotational constraint λ on f' is exemplified in the Fig. 6. As the values of λ enhances the primary velocity is also improves. This is due to an increase inλ, which injects more momentum into the boundary layer and accelerates the fluid. It is seen that velocity of the single CNT is more than hybrid CNTs.

The effect of radiation constraint R_{ad} on thermal profile is shown in the Fig. 7. Improvement in the R_{ad} will extends the thermal delivery. In physical view, implementation in radiation constraint diminishes the k^* which leads to the fact that, the radiative thermal flux indices and radiative heat transfer rates into the fluid will improve as a consequence. The thickness of the thermal boundary layer is noticed due to enhanced radiative thermal transmission. Rosseland's diffusion approach for the given radiation advances the temperature of the liquid. It is observed that thermal distribution is more in case of hybrid CNTs than single CNT.

The discrepancy of concentration profile in the presence of Schmidt number Sc is portrayed in the Fig. 8. The Sc in fluid flow is the ratio of mass and momentum diffusivity. The concentration profile declines as a result of molecular diffusion as the value of Sc falls. The similar variations are observed in the

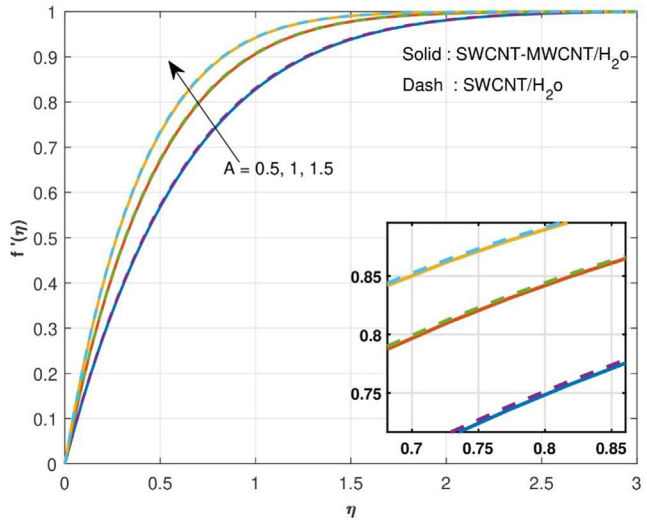

Fig. 2 Change in f' for variation of A.

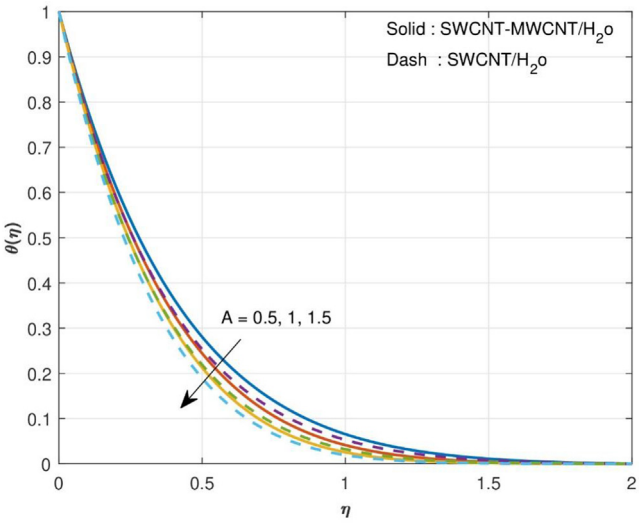

Fig. 4 Change in θ for variation of A.

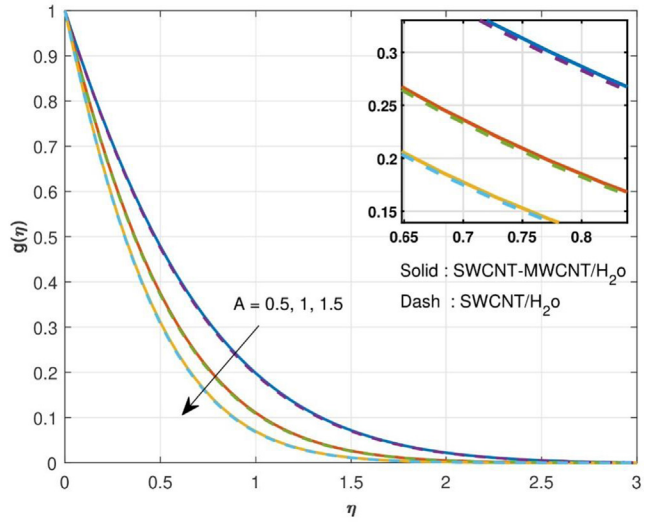

Fig. 3 Change in g for variation of A.

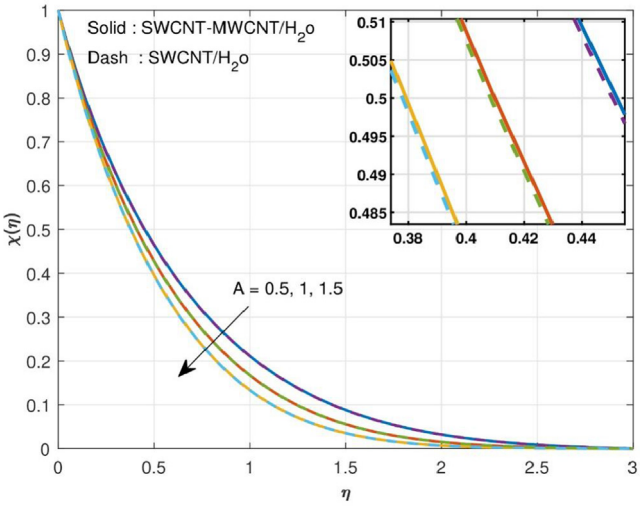

Fig. 5 Change in χ for variation of A.

case of thermophoretic constraint also (see Fig. 9). As τ rises, the temperature gradient shifts, causing nanoparticles to move from a hot to a cool zone. In both the cases, the concentration of hybrid CNTs are more than that of single CNT.

Fig. 10 illustrates the influence of rotational parameter λ on Cf_x for various values of solid volume fractionϕ_2. Rise in the values of ϕ_2 and λ will upsurges the Cf_x This is due to increase in the ϕ_2 and λ will diminishes the boundary layer thickness, results in high surface drag force is seen. The same trend is observed in Cf_z case also (see Fig. 11). The rate of thermal transfer will enhance with enhancement in solid volume fraction and radiation parameter (see Fig. 12). The improvement in ϕ_2 will enhances the boundary layer thickness and improvement in R_{ad} will enhances the Rosseland's diffusion approach. The rate of thermal distribution thus improves. Fig. 13 implies the variation rate of mass transfer in the presence of ϕ_2 and τ parameter. As the values of τ improves, the rate of mass transfer declines due to the presence of temperature gradient.

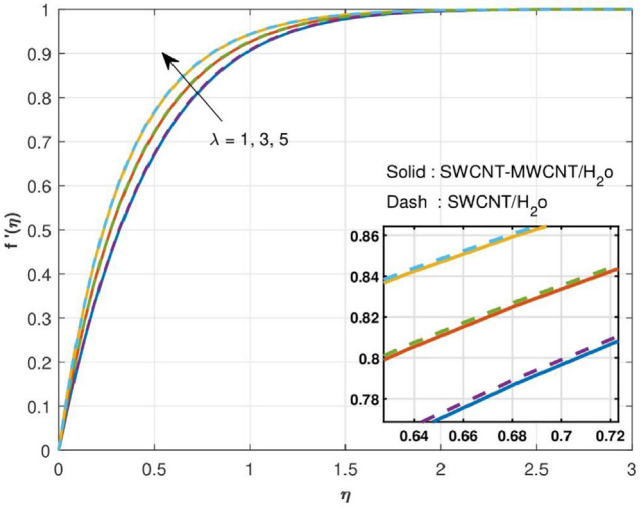

Fig. 6 Change in f' for variation of λ.

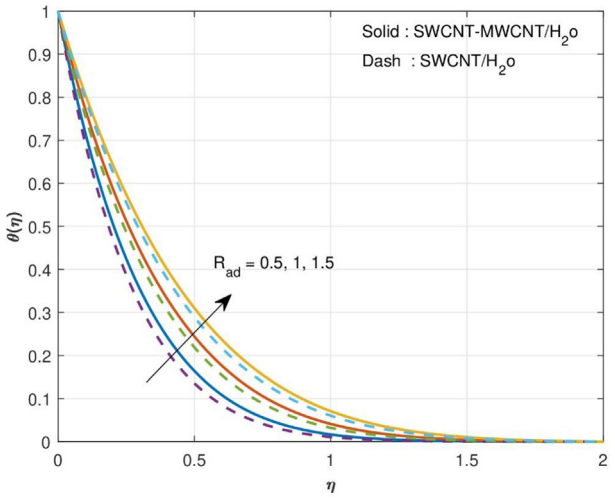

Fig. 7 Change in θ for variation ofR_{ad}.

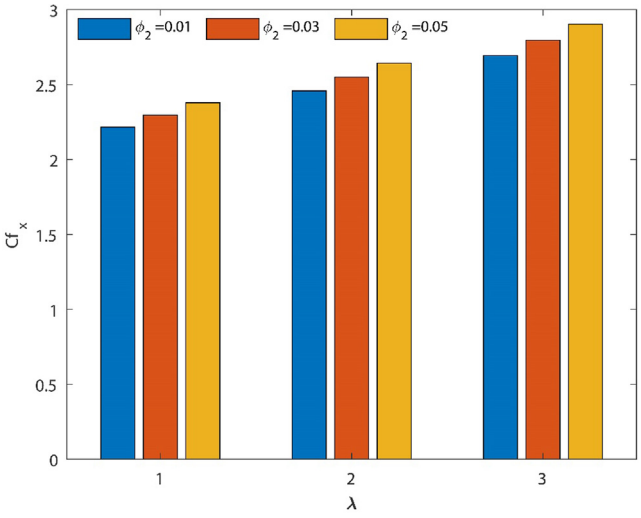

Fig. 10 Variation of Cf_x on λ for change inϕ_2.

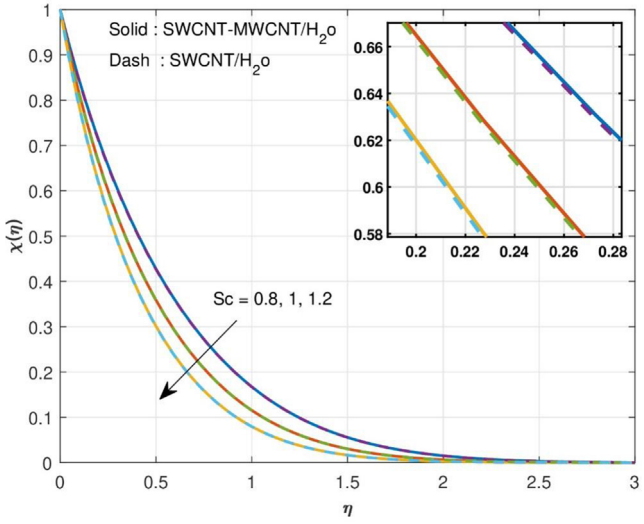

Fig. 8 Change in χ for variation ofSc.

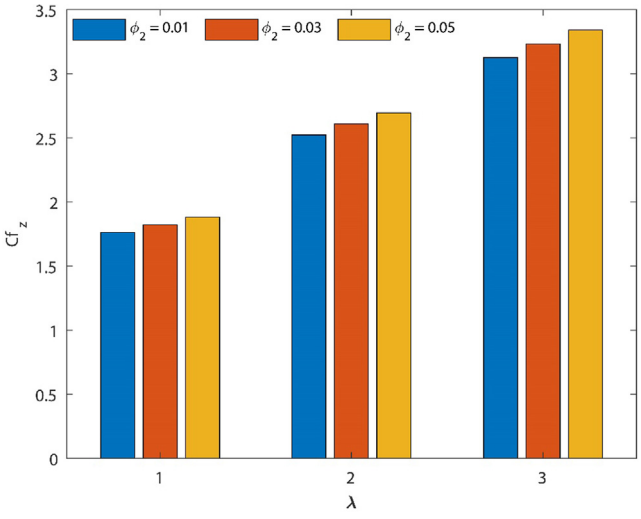

Fig. 11 Variation of Cf_z on λ for change inϕ_2.

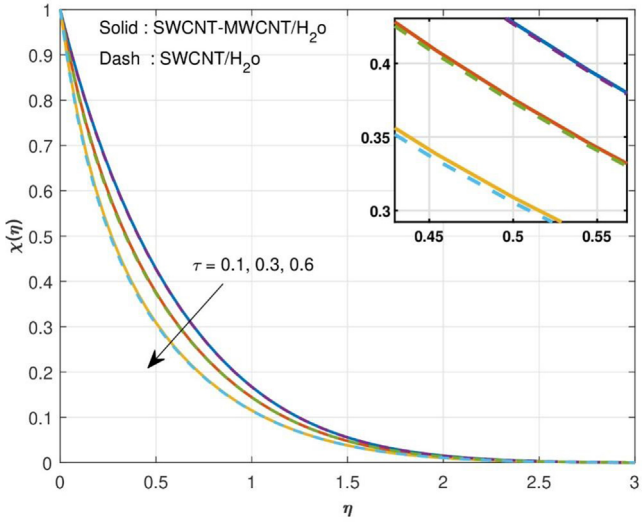

Fig. 9 Change in χ for variation ofτ.

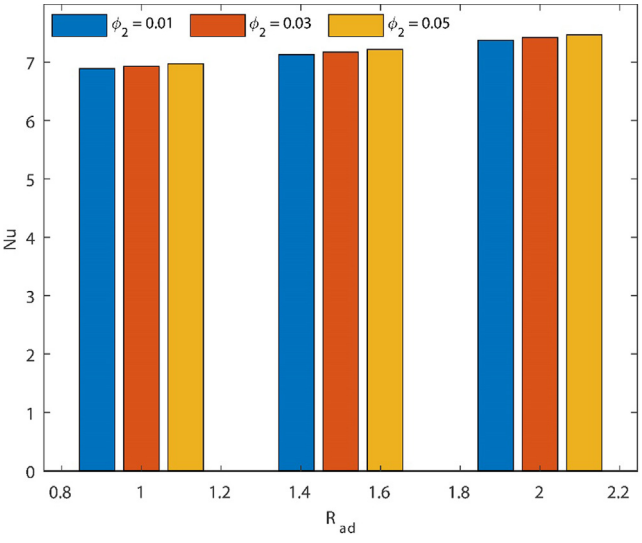

Fig. 12 Variation of Nu on R_{ad} for change inϕ_2.

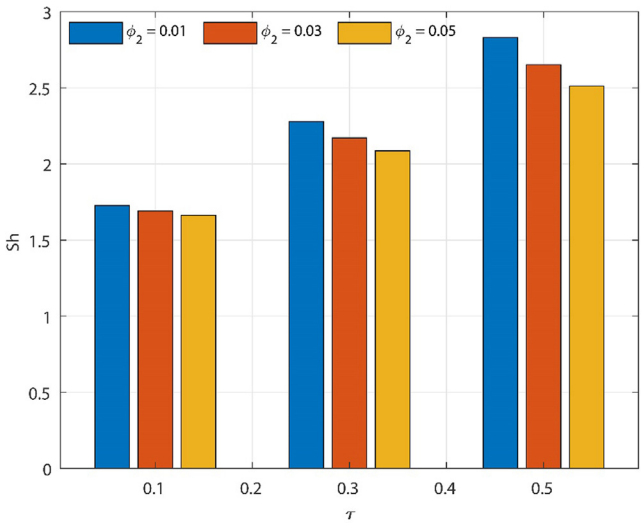

Fig. 13 Variation of Sh on τ for change inϕ_2.

Fig. 14 is drawn to show the streamline pattern in the absence/presence of acceleration constraint.

5. Conclusion

In the current investigation, we discussed the stagnation point hybrid CNTs flow over a rotating sphere in the attendance of thermal radiation (T-R) and thermophoretic particle deposition. The RKF-45 method is used to calculate the flow controlling equations using the bvp4c MATLAB programme. The numerical data is graphed to demonstrate how the different dimensionless parameters change along with their respective profiles. The key discoveries of the current work are as follows:

1. Primary velocity increases as the acceleration constraint is increased, while secondary velocity decreases.
2. Thermal distribution is increases as radiation parameter enhances. Further, hybrid CNTs shows greater thermal performance than single CNT.
3. The primary velocity will improve as the rotational constraint increases.
4. The concentration profile shows declination in the occurrence of thermophoretic particle deposition. Also, concentration is more in hybrid CNTs than that of single CNT.
5. Surface drag force enhances in both Cf_x and Cf_x profiles with upsurge in the solid volume fraction and rotational constraint.
6. Thermal distribution rate improves with escalating the solid volume fraction and radiation constraint whereas mass transfer rate declines in the accurance of thermophoretic constraint.
7. Hybrid CNTs shows greater impact in thermal and concentration profiles while single CNT shows dominant role in velocity profile.

Declaration of Competing Interest

The authors declare that they have no known competing financial interests or personal relationships that could have appeared to influence the work reported in this paper.

References

[1] S.U.S. Choi, J.A. Eastman, Enhancing thermal conductivity of fluids with nanoparticles, Argonne National Lab. (ANL), Argonne, IL (United States), 1995.
[2] G. Rasool, A. Shafiq, S. Hussain, M. Zaydan, A. Wakif, A.J. Chamkha, M.S. Bhutta, Significance of rosseland's radiative process on reactive maxwell nanofluid flows over an isothermally heated stretching sheet in the presence of darcy-

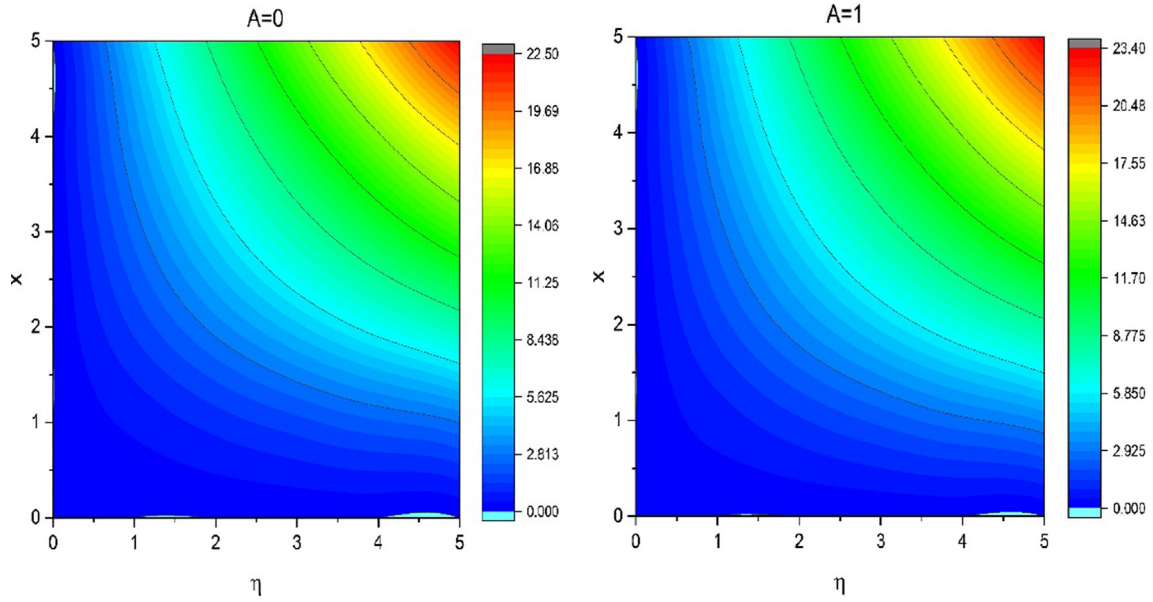

Fig. 14 Streamlines in the absence and presence of$A$.

forchheimer and lorentz forces: towards a new perspective on buongiorno's model, Micromachines. 13 (2022) 368, https://doi.org/10.3390/mi13030368.
[3] J.K. Madhukesh, G.K. Ramesh, E.H. Aly, A.J. Chamkha, Dynamics of water conveying SWCNT nanoparticles and swimming microorganisms over a Riga plate subject to heat source/sink, Alex. Eng. J. 61 (3) (2022) 2418–2429.
[4] U. Khan, S. Ahmad, A. Hayyat, I. Khan, K.S. Nisar, D. Baleanu, On the Cattaneo-Christov Heat Flux Model and OHAM analysis for three different types of nanofluids, Applied Sciences. 10 (2020) 886.
[5] P. Michael Joseph Stalin, T.V. Arjunan, M.M. Matheswaran, P. Manoj Kumar, N. Sadanandam, Investigations on thermal properties of CeO2/water nanofluids for heat transfer applications, Mater. Today Proc. 47 (2021) 6815–6820.
[6] J.K. Madhukesh, G.K. Ramesh, B.C. Prasannakumara, S.A. Shehzad, F.M. Abbasi, Bio-Marangoni convection flow of Casson nanoliquid through a porous medium in the presence of chemically reactive activation energy, Appl. Math. Mech. 42 (8) (2021) 1191–1204.
[7] G.K. Ramesh, J.K. Madhukesh, B.C. Prasannakumara, S.A. Shehzad, F.M. Abbasi, Thermodynamics examination of Fe3O4-CoFe2O4/Water + EG nanofluid in a heated plate: crosswise and stream-wise aspects, Arab J Sci Eng 47 (7) (2022) 8351–8360.
[8] S. Das, R.N. Jana, O.D. Makinde, MHD Flow of Cu-Al2O3/Water Hybrid Nanofluid in Porous Channel: analysis of entropy generation, defect and diffusion, Forum. 377 (2017) 42–61.
[9] Sajad. Salehi, Amin. Nori, Kh. Hosseinzadeh, D.D. Ganji, Hydrothermal analysis of MHD squeezing mixture fluid suspended by hybrid nanoparticles between two parallel plates, Case Studies in Thermal Engineering. 21 (2020) 100650.
[10] M.K. Nayak, V.S. Pandey, S. Shaw, O.D. Makinde, K.M. Ramadan, M. Ben Henda, I. Tlili, Thermo-fluidic significance of non Newtonian fluid with hybrid nanostructures, Case Studies, Therm. Eng. 26 (2021) 101092.
[11] S. Shaw, S.S. Samantaray, A. Misra, M.K. Nayak, O.D. Makinde, Hydromagnetic flow and thermal interpretations of Cross hybrid nanofluid influenced by linear, nonlinear and quadratic thermal radiations for any Prandtl number, Int. Commun. Heat Mass Transfer 130 (2022) 105816, https://doi.org/10.1016/j.icheatmasstransfer.2021.105816.
[12] K. Hosseinzadeh, M.R. Mardani, S. Salehi, M. Paikar, M. Waqas, D.D. Ganji, Entropy generation of three-dimensional Bödewadt flow of water and hexanol base fluid suspended by Fe3O4 and MoS2 hybrid nanoparticles, Pramana - J Phys. 95 (2021) 57.
[13] V. Puneeth, S. Manjunatha, O.D. Makinde, B.J. Gireesha, Bioconvection of a radiating hybrid nanofluid past a thin needle in the presence of heterogeneous-homogeneous chemical reaction, J. Heat Transfer 143 (2021).
[14] S. Hosseinzadeh, K.h. Hosseinzadeh, A. Hasibi, D.D. Ganji, Thermal analysis of moving porous fin wetted by hybrid nanofluid with trapezoidal, concave parabolic and convex cross sections, Case Studies in Thermal Eng. 30 (2022), https://doi.org/10.1016/j.csite.2022.101757 101757.
[15] Z. Hussain, T. Muhammad, Simultaneous influence of hall and wall characteristics in peristaltic convective carbon-water flow subject to soret and dufour effects, Arab. J. Sci. Eng. 46 (3) (2021) 2033–2046.
[16] M.S. Iqbal, I. Mustafa, I. Riaz, A. Ghaffari, W.A. Khan, Influence of carbon nanotubes on heat transfer in MHD nanofluid flow over a stretchable rotating disk: a numerical study, Heat Transf. 50 (1) (2021) 619–637.
[17] M. Gholinia, K.h. Hosseinzadeh, D.D. Ganji, Investigation of different base fluids suspend by CNTs hybrid nanoparticle over a vertical circular cylinder with sinusoidal radius, Case Studies in Thermal Eng. 21 (2020) 100666.
[18] K.h. Hosseinzadeh, S.o. Roghani, A.R. Mogharrebi, A. Asadi, D.D. Ganji, Optimization of hybrid nanoparticles with mixture fluid flow in an octagonal porous medium by effect of radiation and magnetic field, J Therm Anal Calorim. 143 (2) (2021) 1413–1424.
[19] B.J. Gireesha, B. Nagaraja, N. Srikantha, N.G. Rudraswamy, A. Felicita, Magnetically propelled Carreau fluid flow over penetrable sensor surface influenced by thermal radiation, Joule heating and heat generation, Commun. Theor. Phys. 74 (2022) 025002.
[20] K.h. Hosseinzadeh, S. Salehi, M.R. Mardani, F.Y. Mahmoudi, M. Waqas, D.D. Ganji, Investigation of nano-Bioconvective fluid motile microorganism and nanoparticle flow by considering MHD and thermal radiation, Inf. Med. Unlocked 21 (2020) 100462.
[21] N.A. Shah, A. Wakif, E.R. El-Zahar, S. Ahmad, S.-J. Yook, Numerical simulation of a thermally enhanced EMHD flow of a heterogeneous micropolar mixture comprising (60%)-ethylene glycol (EG), (40%)-water (W), and copper oxide nanomaterials (CuO), Case Stud. Therm. Eng. 35 (2022) 102046, https://doi.org/10.1016/j.csite.2022.102046.
[22] H.L. Green, W.R. Lane, Particulate Clouds: Dusts, Smokes and Mists. Their Physics and Physical Chemistry and Industrial and Environmental Aspects, Part. Clouds Dusts Smokes Mists Their Phys. Phys. Chem. Ind. Environ. Asp. (1957).
[23] N.A, Fuchs, The Mechanics of Aerosols, Pergamon Press, Oxford, 1964.
[24] S.L. Goren, Thermophoresis of aerosol particles in the laminar boundary layer on a flat plate, J. Colloid Interface Sci. 61 (1) (1977) 77–85.
[25] C.S.K. Raju, N.A. Ahammad, K. Sajjan, N.A. Shah, S.-J. Yook, M.D. Kumar, Nonlinear movements of axisymmetric ternary hybrid nanofluids in a thermally radiated expanding or contracting permeable Darcy Walls with different shapes and densities: simple linear regression, Int. Comm. Heat Mass 135 (2022) 106110, https://doi.org/10.1016/j.icheatmasstransfer.2022.106110.
[26] N. Shu-Bo Chen, M. Shahmir, Y.-L. Ramzan, A.A. Sun, M.Y. M. Aly, Thermophoretic particle deposition in the flow of dual stratified Casson fluid with magnetic dipole and generalized Fourier's and Fick's laws, Case Stud, Therm. Eng. 26 (2021) 101186.
[27] B.M. Shankaralingappa, J.K. Madhukesh, I.E. Sarris, B.J. Gireesha, B.C. Prasannakumara, Influence of thermophoretic particle deposition on the 3D flow of sodium alginate-based casson nanofluid over a stretching sheet, Micromachines. 12 (2021) 1474.
[28] T. Gul, B. Ali, W. Alghamdi, S. Nasir, A. Saeed, P. Kumam, S. Mukhtar, W. Kumam, M. Jawad, Mixed convection stagnation point flow of the blood based hybrid nanofluid around a rotating sphere, Sci. Rep. 11 (2021) 7460.
[29] A. Malvandi, The unsteady flow of a nanofluid in the stagnation point region of a time-dependent rotating sphere, Therm. Sci. 19 (5) (2015) 1603–1612.
[30] D. Anilkumar, S. Roy, Self-similar solution of the unsteady mixed convection flow in the stagnation point region of a rotating sphere, Heat Mass Transf. 40 (6-7) (2004), https://doi.org/10.1007/s00231-003-0447-7.
[31] A. Mahdy, A.J. Chamkha, H.A. Nabwey, Entropy analysis and unsteady MHD mixed convection stagnation-point flow of Casson nanofluid around a rotating sphere, Alexandria Eng. J. 59 (3) (2020) 1693–1703.
[32] A. Sarkar, P.K. Kundu, Framing the upshot of Hall current on MHD unsteady nanofluid flow from a rotating spherical body in presence of solar radiation, Int. J. Ambient Energy. (2021) 1–11.
[33] M. Epstein, G.M. Hauser, R.E. Henry, Thermophoretic deposition of particles in natural convection flow from a vertical plate, J. Heat Transfer 107 (1985) 272–276.

[34] G.K. Ramesh, J.K. Madhukesh, Activation energy process in hybrid CNTs and induced magnetic slip flow with heat source/sink, Chin. J. Phys. 73 (2021) 375–390.

[35] T. Hayat, S.A. Khan, A. Alsaedi, Q.M.Z. Zai, Computational analysis of heat transfer in mixed convective flow of CNTs with entropy optimization by a curved stretching sheet, Int. Commun. Heat Mass Transfer 118 (2020) 104881.